Bull Volcanol (2014) 76:831
DOI 10.1007/s00445-014-0831-9

RESEARCH ARTICLE

The large late-glacial Ho eruption of the Hudson volcano, southern Chile

D. Weller · C. G. Miranda · P. I. Moreno · R. Villa-Martínez · C. R. Stern

Received: 19 December 2013 / Accepted: 3 May 2014

Abstract Lakes formed in the Aysén region of southern Chile after the retreat of mountain glaciers, established by ~17,900 calendar years before present (cal years BP) or earlier, contain numerous late-glacial and Holocene tephra layers derived from >70 eruptions of the volcanoes in the region, including Hudson, the southernmost in the Andean Southern Volcanic Zone (SVZ). Sediment cores from seven of these lakes contain an unusually thick late-glacial age tephra layer, which based on its distribution and bulk trace-element composition was derived from a large explosive eruption of Hudson volcano between 17,300 and 17,440 cal years BP and is termed Ho. In 13 cores from six of these lakes, each located ~100 km generally northeast of Hudson, the Ho tephra layer ranges between 50 and 88 cm in thickness, and contains pumice grains up to 2 cm in maximum diameter. Comparison with three previously documented large explosive Holocene Hudson eruptions (H1 at 7,750 cal years BP, H2 at 3,920 cal years BP, and H3 in 1991 AD) suggests that Ho was larger, with an estimated tephra volume of >20 km^3, the largest post-glacial eruption documented for any volcano in the southern Andes and most likely responsible for the formation of the Hudson caldera. In total, Hudson has erupted ≥45 km^3 of pyroclastic material in the last ~17,500 years, making it the most productive volcano in the southern Andes in terms of the total volume erupted since the beginning of deglaciation in the region. Chemical stratification is not seen in the waterlain Ho tephra, but these deposits are bi-modal, consisting of a much greater proportion of dark glassy basaltic-trachyandesite dense fragments and pumice, with glasses which range between 55 and 59 wt.% SiO_2, along with volumetrically less-significant lighter-colored trachydacite pumice, with glass of 66 wt.% SiO_2. In contrast, H1 products are trachyandesitic in composition, H2 ones are more felsic than H1, being composed essentially of trachydacite, and although H3 1991 AD again produced tephra of bi-modal compositions, it erupted a much smaller proportion of mafic compared to felsic material than did Ho. Thus, the repetitive large explosive eruptions of Hudson volcano have evolved to progressively less-mafic overall compositions from late-glacial to historic times, and their volumes have decreased. Sr-isotopic composition of bulk samples of the most mafic dense glass and most felsic pumice components of the Ho tephra, as well as samples from other Hudson eruptions, which overall range from 51 to 66 wt.% SiO_2, with 525 to 227 ppm Sr, are all similar (0.70444± 0.00007), indicating that crystal-liquid fractionation rather than crustal assimilation was the main process responsible for these chemical variations.

Keywords Hudson volcano · Explosive volcanism · Andean volcanism · Chile

Editorial responsibility: M.L. Coombs

D. Weller · C. R. Stern (✉)
Department of Geological Sciences, University of Colorado, Boulder, CO 80309-0399, USA
e-mail: Charles.Stern@colorado.edu

C. G. Miranda · P. I. Moreno
Instituto de Ecología y Biodiversidad, Departamento de Ciencias Ecológicas, Universidad de Chile, Casilla 653, Santiago, Chile

R. Villa-Martínez
Centro de Estudios del Cuaternario de Fuego-Patagonia y Antartica (Fundación CEQUA), 21 de Mayo 1690, Casilla 737, Punta Arenas, Chile

Introduction

The southern portion of the Andean Southern Volcanic Zone (SVZ, Fig. 1; Stern 2004; Stern et al. 2007) is composed of several large composite volcanoes, including Melimoyu, Mentolat, Maca, Cay, and Hudson, and also many (>15; Fig. 1) small monogenetic mafic cones along the Liquiñe-

Published online: 22 May 2014

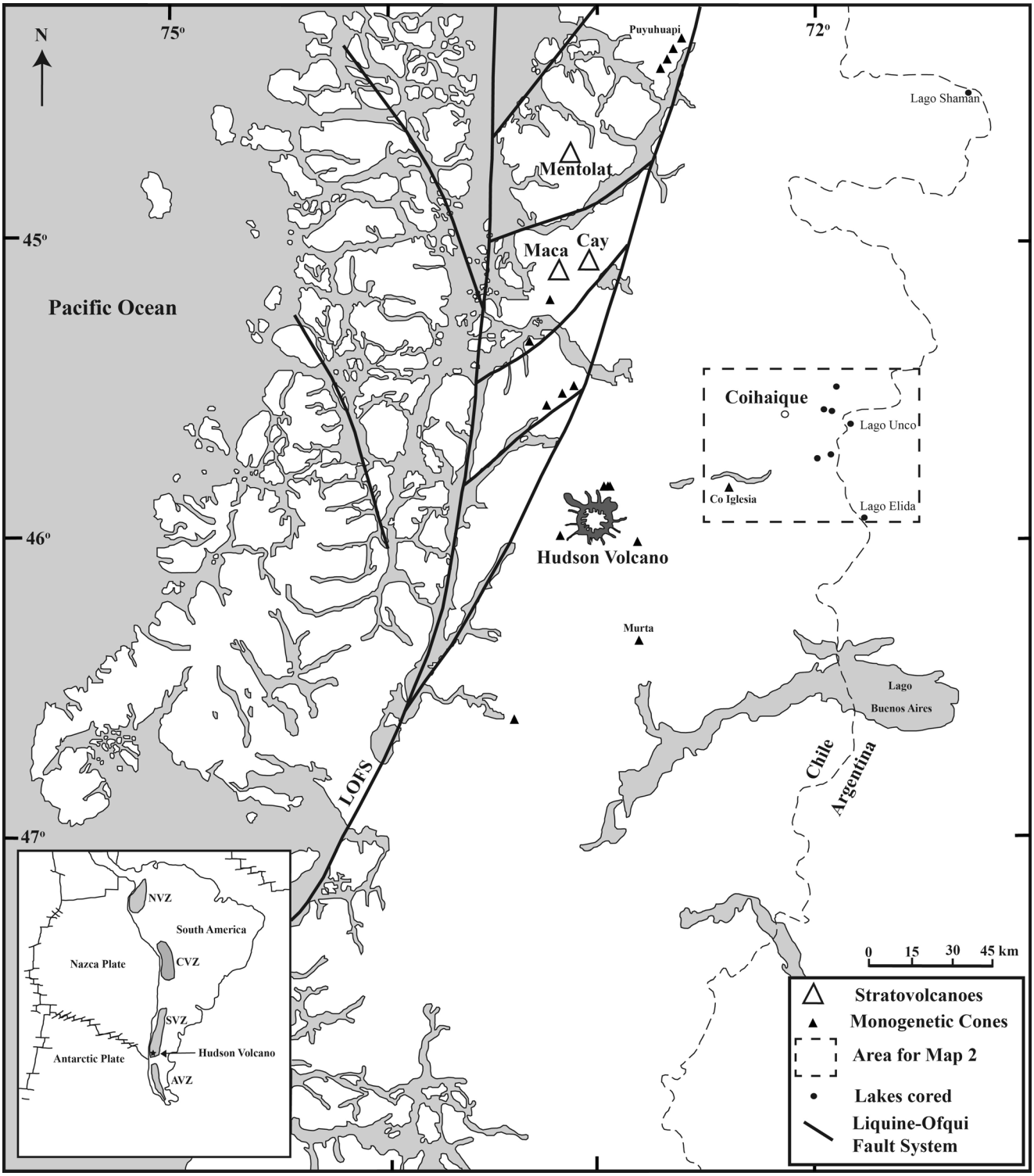

Fig. 1 Map of southernmost portion of the SVZ showing the location of Hudson, Maca, Cay, and Mentolat volcanoes. Also shown are the locations of some of the >15 monogenetic centers along the Liquiñe-Ofqui Fault System (LOFS) and surrounding Hudson (Gutiérrez et al. 2005). The *boxed area* encloses the lakes from which cores were obtained (Fig. 2; Miranda et al. 2013). Lago Shaman (de Porras et al. 2012) lies further to the northeast

Ofqui Fault System (LOFS; Gutiérrez et al. 2005). Lacustrine sediment cores, from seven lakes formed in this region of Chile (Figs. 1 and 2) after the initiation of the retreat of mountain glaciers, which started by at least ~17,900 calendar years before present (cal years BP) (Miranda et al. 2013), each contain multiple tephra layers derived from an integrated total

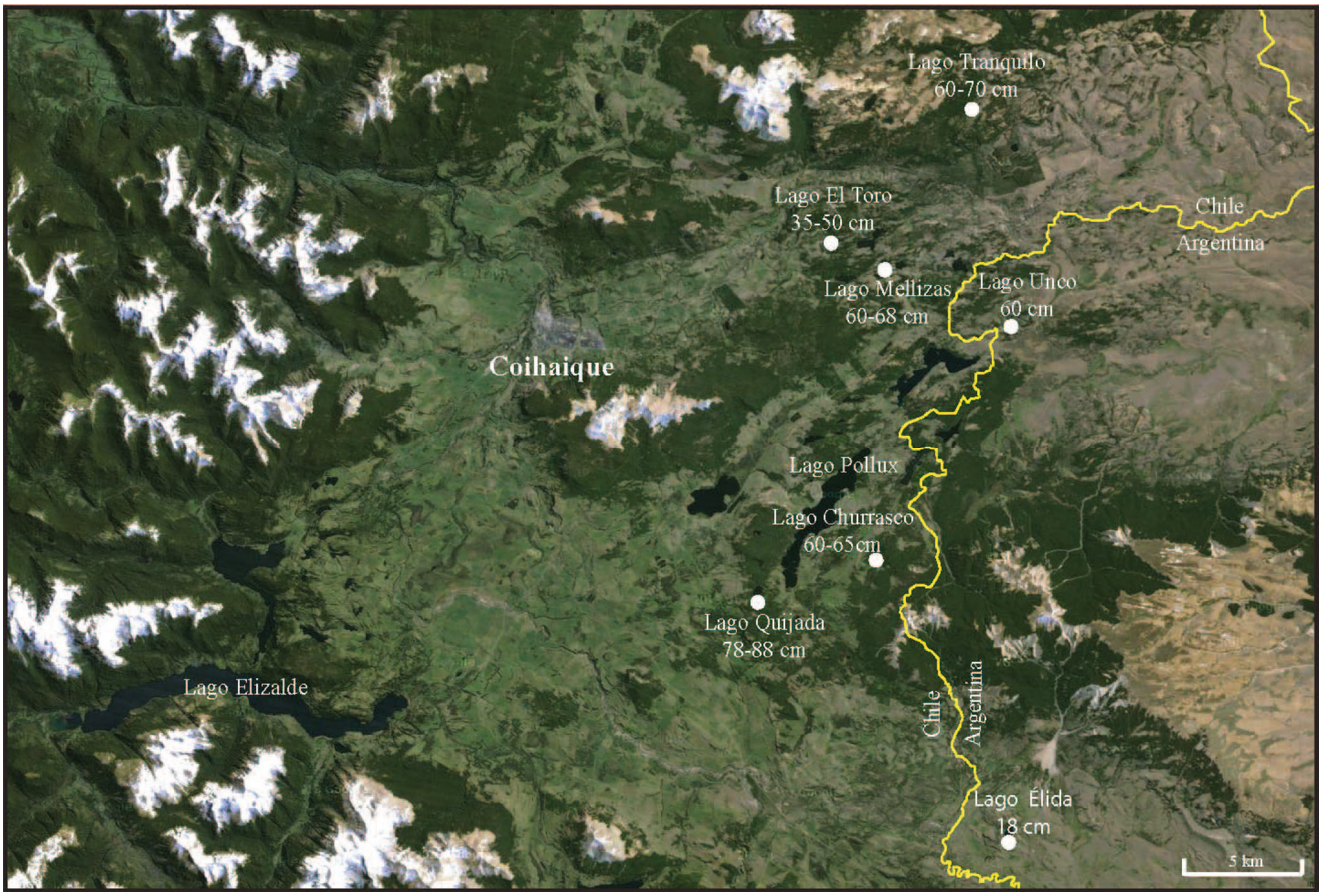

Fig. 2 Google Earth image showing the location of the seven lakes from which the cores (Figs. 3 and 4) discussed in the text were taken and the thickness range for the Ho deposits in each lake (Table 2)

of >70 explosive eruptions of these volcanoes (Figs. 3 and 4). These eruptions span the period of climate change at the transition from the glacial to the post-glacial warm period and extend through the Holocene.

Specific source volcanoes for some of the tephra layers in these cores have been identified from their trace-element chemistry. Based on their chemical characteristics (Fig. 5) and their stratigraphic depth in the cores, some of the previously identified and dated large explosive eruptions of Hudson, such as H2 at ~3,920 cal years BP (Naranjo and Stern 1998), and of Mentolat, such as MEN1 at 7,560 cal years BP (Naranjo and Stern 2004; Stern et al. 2013), are represented by tephra in these cores (Fig. 3).

Hudson (45°54′S; 72°58′W), which is the southernmost volcanic center in the SVZ, has had three large explosive eruptions during the Holocene (Stern 1991, 2008; Scasso et al. 1994; Naranjo and Stern 1998; Kratzmann et al. 2009, 2010). Fifteen sediment cores from the seven lakes each contain an unusually thick late-glacial age tephra layer (Tables 1 and 2; Figs. 3 and 4) resulting from a very large explosive eruption, which based on both its bulk trace-element composition (Fig. 5) and distribution (Fig. 6), was derived from Hudson volcano and is termed Ho (Weller et al. 2013). Here, we characterize some of the physical and chemical features of the late-glacial Ho eruptive products and make an assessment of the total eruptive volume of this and other explosive eruptions of Hudson since the beginning of deglaciation in southern Chile.

Geologic/tectonic setting

Hudson volcano is the southernmost volcano in the Andean Southern Volcanic Zone (SVZ; 33–46°S; Stern 2004; Stern et al. 2007). Volcanism in this section of the Andean cordillera is the result of subduction of the Nazca Plate under the South American continent (Fig. 1). Further to the south is the Austral Volcanic Zone (AVZ; Stern and Kilian 1996), in which volcanism is the result of the subduction of the Antarctic Plate underneath the southern portion of the South American Plate. In between the AVZ and Hudson is a ~350-km gap in the active volcanic arc that lies just south of where the Chile Rise, an active spreading center that separates the Antarctic and Nazca Plates, has been subducted under the South American Plate (Cande and Leslie 1986). Marine geophysical data

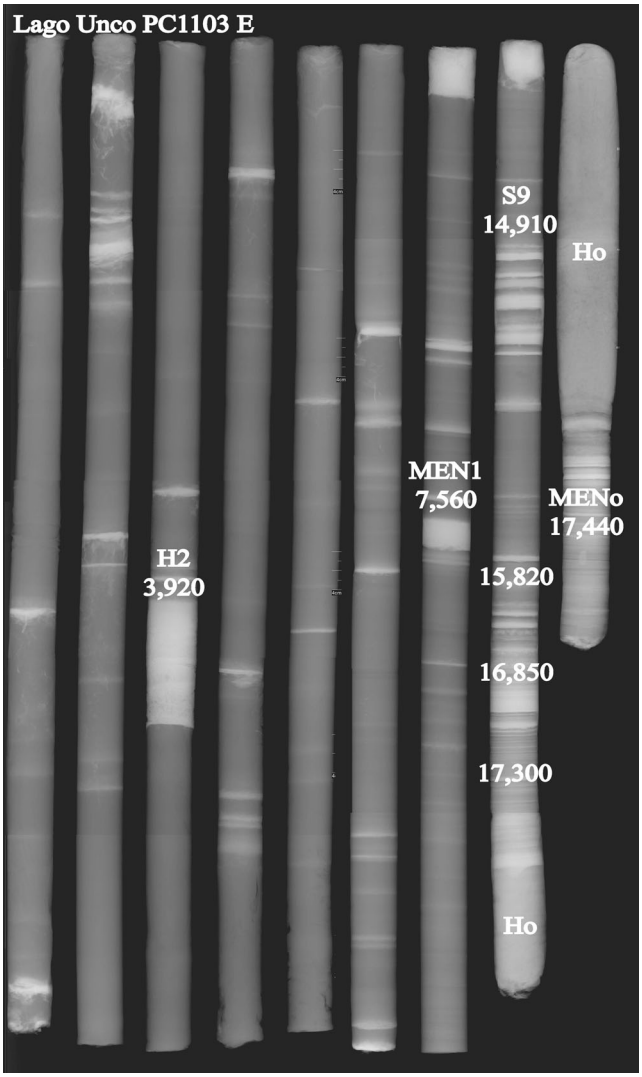

Fig. 3 X-ray image of the 8.5×1 m sections of core extracted from Lago Unco, >100 km east of Hudson volcano (Figs. 1 and 2). The 74 different tephras in this core appear as *white layers* due to their higher density compared to the predominantly organic lake sediments in which they are preserved. The large late-glacial Ho tephra is 60-cm thick, extending from core section 8 at 78 cm to section 9 at 38 cm, and contains pumice up to >2 cm in diameter. The inferred age of Ho is constrained in this core by dates in the organic rich sediments overlying and underlying the Ho tephra as between 17,300 and 17,440 cal years BP in age (Table 1; Miranda et al. 2013). These ages are consistent with it underlying a late-glacial tephra sequence S9 dated as <14,910 cal years BP (Miranda et al. 2013)

indicate that the Chile Rise first collided with the Chile Trench near Tierra del Fuego and has migrated north along the continental margin since 15–20 Ma to its current location (Cande and Leslie 1986; Nelson et al. 1994).

Cembrano et al. (1996) suggest that there is a strong connection between the arc-parallel Liquiñe-Ofqui Fault System (LOFS; Fig. 1) and the location of the volcanic centers of the SVZ. The LOFS results from a combination of oblique subduction of the Nazca Plate and the impingement of the Chile Rise against the continent. Most of the southern SVZ volcanoes are located along or to the west of the LOFS. Hudson volcano, in contrast, is situated approximately 30 km east of this fault zone (Naranjo and Stern 1998). Numerous monogenetic mafic cinder cones are also roughly aligned along the LOFS trend (Fig. 1; Gutiérrez et al. 2005), and others surround Hudson as well.

The Quaternary volcanoes of the southern SVZ are located on a portion of the Northern Patagonian Batholith composed of mainly tonalites and granodiorites (Pankhurst et al. 1999; D'Orazio et al. 2003; Gutiérrez et al. 2005). This Cretaceous to late Miocene intrusive complex, which is ~1,000 km in length and extends across the length of the southern SVZ (41°S–52°S), formed by episodic magmatic events over a 125 Myr time interval (Pankhurst et al. 1999).

The magmas produced by the southern SVS volcanoes are generally high-Al_2O_3 basalts and basaltic andesites (Futa and Stern 1988; López-Escobar et al. 1993; D'Orazio et al. 2003), with only minor andesites, dacites, and rhyolites. Hudson generates magmas which are compositionally distinct from the other southern SVZ volcanic centers such as Mentolat (Fig. 5), Maca, and Cay. Analyzed samples from Hudson range from basalts to trachydacites with high TiO_2, FeO, Na_2O, and K_2O relative to rocks of similar silica content erupted from other volcanic centers in the southern SVZ (Futa and Stern 1988; Stern 1991, 2008; López-Escobar et al. 1993; Naranjo and Stern 1998; D'Orazio et al. 2003; Gutiérrez et al. 2005; Kratzmann et al. 2009, 2010). Hudson's extrusive rocks are also rich in incompatible trace elements, which include LILE, REE, and HFSE, compared to samples from other southern SVZ and AVZ volcanoes with similar silica content (Stern 1991, 2008; Naranjo and Stern 1998).

Hudson eruptions

The Hudson caldera was first identified as a volcano only after a small Plinian eruption and lahar in 1971 (Tobar 1972; Fuenzalida and Espinosa 1974; Fuenzalida 1976; Cevo 1978; Best 1989, 1992). Hudson erupted as recently as October 2011 and K-Ar dates indicate that this volcano has been active since 1 Ma or before (Orihashi et al. 2004). The most recent large explosive eruption from Hudson (H3 in 1991 AD) occurred on August 8, 1991. It began with an initial phreatomagmatic event (phase 1) which erupted through a 400-m crater and a 4-km-long fissure in the northwestern portion of the caldera (Naranjo 1991; Naranjo et al. 1993; Scasso et al. 1994; Kratzmann et al. 2009, 2010; Wilson et al. 2011, 2012). The paroxysmal phase (phase 2) began on the 12th of August with a Plinian style eruption from an 800-m-wide crater located in the southwestern portion of the caldera. This phase of the eruption continued on and off for 3 days before ceasing on the 15th of August. The tephra fallout from

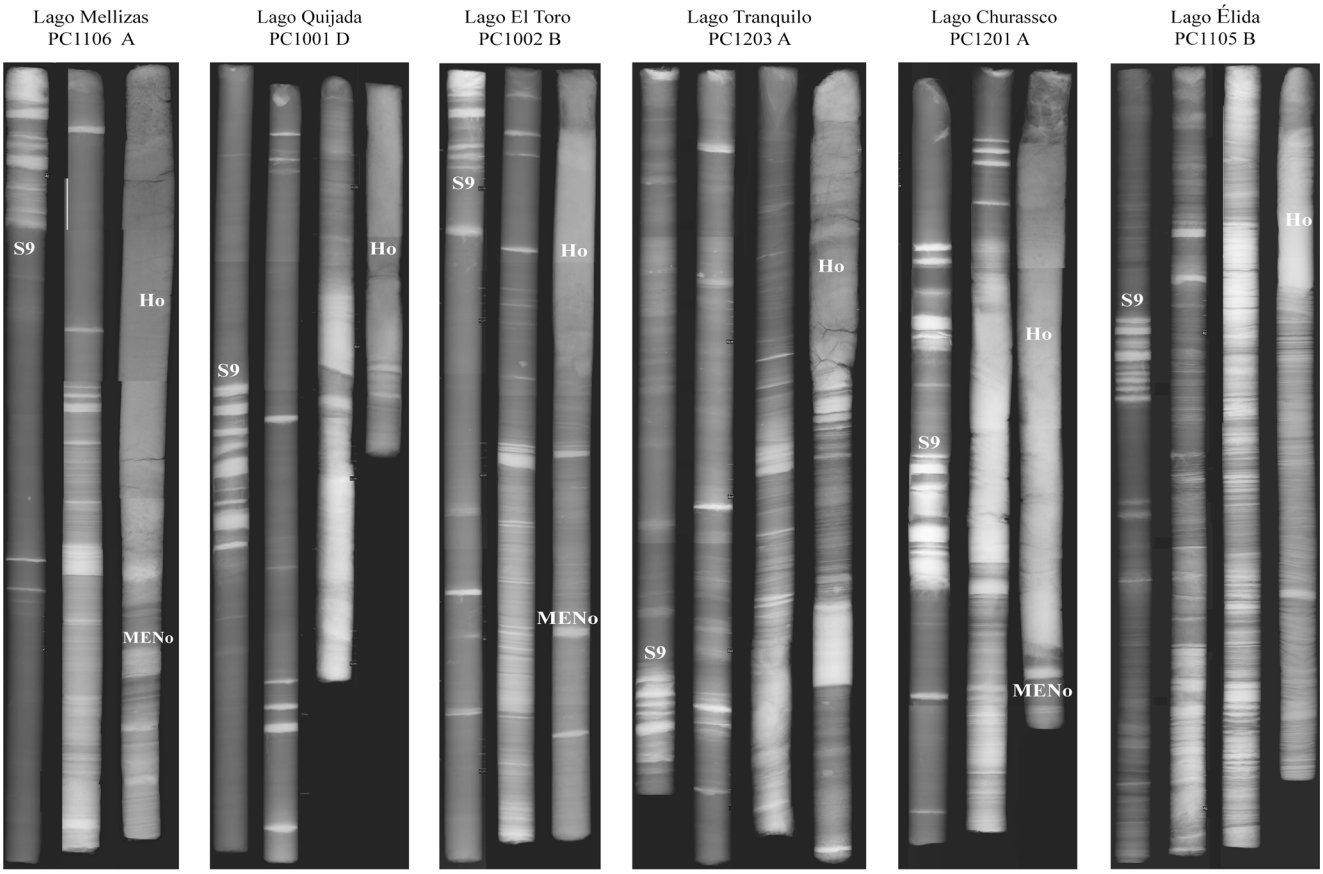

Fig. 4 X-ray images for six of the other lakes where the Ho tephra has been observed. The large late-glacial Hudson eruption is labeled Ho, with the sequence of nine (S9) closely spaced eruptions and MENo as reference deposits for each core. Each section of each core is approximately 1-m long and 4-cm wide

phase 2 was dispersed in an ESE direction covering a narrow, elongated sector of southern Patagonia (Scasso et al. 1994; Wilson et al. 2011, 2012). This eruption produced a volume of at least 4 km^3 of material, but the overall volume is likely to have been larger because tephra was also deposited into the sea. Tephra from this eruption ranges in composition from basalt and basaltic-andesite during phase 1 to trachyandesite and trachydacite during phase 2, with a distinct gap between 54 and 60 wt.% SiO_2 separating the two phases (Kratzmann et al. 2009, 2010). Furthermore, Kratzmann et al. (2009) observed a trend of progressive decrease in SiO_2 content of the eruptive products during the second phase of the eruption. The abrupt transition from basalt/basaltic-andesite (51 to 54 wt.% SiO_2) erupted in the first phase to trachyandesite and trachydacite (60 to 65 wt.% SiO_2) during the second phase and the progressive decrease in SiO_2 during the second phase have been attributed to a combination of magma mixing and fractional crystallization (Kratzmann et al. 2009, 2010).

Soil and sediment sections exposed east and the southeast of the Hudson volcanic center in river and road cuts, as well as in excavated trenches, preserve pyroclastic fallout deposits that were derived from nine explosive Holocene eruptions of Hudson, including two very large ones (Naranjo and Stern 1998). The younger of the two large events (H2) occurred at approximately 3,920 cal years BP, and the older (H1) eruption occurred approximately 7,750 cal years BP (Stern 2008; Prieto et al. 2013). Based on the isopach maps for tephra from these eruptions, Naranjo and Stern (1998) determined that both the H1 and H2 eruptions generated greater volumes of ejected material than did the H3 eruption in 1991 or the 1932 Quizapu eruption (9.5 km^3; Hildreth and Drake 1992). Using radiocarbon age constraints and petrochemical data, Stern (1991, 2008) suggested that grey-green tephra layers in southernmost Patagonia, originally termed Tephra II by Auer (1974), are distal deposits of the H1 eruption derived from Hudson. These form >10-cm-thick tephra deposits in Tierra del Fuego, and this eruption may have had a significant impact on the prehistoric people living on this island (Prieto et al. 2013). Based on the proximal and distal maximum isopachs for the H1 tephra, Stern (1991, 2008) estimated that this eruption ejected >18 km^3 of material. The chronology established by Naranjo and Stern (1998) shows that the recurrence interval between explosive eruptions of Hudson is irregular, but that the three largest Holocene explosive events (H1, H2, and H3 in 1991 AD) are relatively regularly spaced at 3,870±40 years.

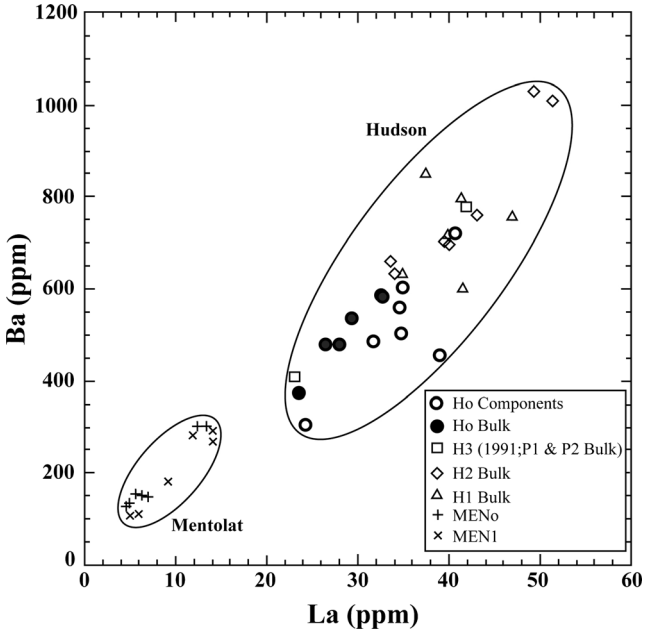

Fig. 5 La versus Ba plot showing the fields occupied by the different eruptive products from Hudson (Ho from Tables 3 and 4; H3 in 1991 AD from Kratzmann et al. 2009 and 2010; H1 and H2 from Naranjo and Stern 1998) and Mentolat Volcano (Naranjo and Stern 2004; Stern et al. 2013). Hudson eruptive products are elevated in LIL, HFSE, and REE compared to Mentolat and other southern SVZ tephras

Although Naranjo and Stern (1998) did not observe any early Holocene or late-glacial tephra, Haberle and Lumley (1998) documented two late-glacial tephra deposits in lake sediments on Peninsula Taitao, 150 km southwest of the volcano. Radiocarbon dating of these deposits yielded ages of 14,560 cal years BP for eruption HW1 and 13,890 cal years BP for eruption HW2 (Haberle and Lumley 1998).

Methods

Multiple sediment cores were obtained, using a 5-cm-diameter modified Livingstone piston corer (Wright 1967), from seven small lakes within spatially limited watershed basins selected to minimize the amount of inorganic sediment deposited in the lakes. X-ray images of the cores (Figs. 3 and 4) were taken to allow for better visual identification of the tephra deposits and to provide a means of stratigraphic correlation of the tephra layers between the cores. The white layers in these images are the denser lithologies, often tephra deposits, and the darker layers are less dense organic-rich lacustrine sediments. The stratigraphic position of the Ho tephra layer, combined with several other key marker tephra deposits which were identified in the multiple cores, allowed for correlation of this deposit within the cores. The chronology of the tephra in the cores is controlled by AMS radiocarbon dates of organic material in the sediments (Table 1; Miranda et al. 2013) and chronostratigraphic correlation of tephra layers. Radiocarbon dates were converted to calendar years before present (cal years BP) using the CALIB 5.01 program (Stuiver et al. 1998).

Once identified, the individual tephra deposits were extracted from the cores by removing approximately half of the deposit with a knife. Several of the Ho tephra layers were sufficiently large to sample at discrete 10-cm intervals to assess if any vertical stratification is present within the deposits. The tephra samples were washed to remove any organic matter, and then dried and sieved to remove any coarse fraction material not volcanic in origin. Within the Ho deposits, several different eruptive phases were apparent based on particle color and morphology. Based on these characteristics, the different particle types were hand-picked out of the deposit. Thin sections of these particles were prepared for examination under a petrographic microscope in order to determine tephra morphology and mineral phases present.

Trace-element compositions for 2–10 g of both bulk tephra samples and hand-picked pumice and dense glass fragments were determined using an ELAN D CR ICP-MS. The major element compositions of pumice glass, dense glass, and mineral phases were determined using a Jeol JXA-733 Electron Microprobe. A 5–10-μm beam, 15 KV accelerating potential,

Table 1 Age constrains for the Ho tephra deposits from Miranda et al. (2013)

Lake	Laboratory code	Core	Core depth (cm)	^{14}C years BP	cal year BP (range 2σ)	median cal year BP
<Ho						
Lago Unco	UCIAMS-122978	PC1103ET8	1,419–1,420	13,430±50	16,204–16,875	16,612
Lago Unco	CAMS-159614	PC1103ET8	1,423–1,424	13,720±45	16,692–17,018	16,850
Lago Mellizas	CAMS-159606	PC1106AT6	1,348–1,349	13,810±110	16,691–17,178	16,914
Lago Quijada	CAMS-159607	PC1001DT10	1,664–1,665	14,220±45	16,992–17,595	17,299
>Ho						
Lago Unco	CAMS-159613	PC1103ET9	1,517–1,518	14,345±45	17,132–17,788	17,443
Lago Mellizas	UCIAMS-122999	PC1106BT7	1,452–1,453	14,670±45	17,573–18,368	17,847
Lago Quijada	CAMS-154860	PC1001ET9	1,685–1,686	14,735±30	17,648–18,432	17,920
Lago Mellizas	UCIAMS-123030	PC1106BT7	1,457–1,458	14,800±90	17,661–18,509	18,014

Table 2 Thickness (in cm) of the Ho and H2 tephra deposits in lake cores from south Chile

		Ho			H2			
Lake	Core	Thickness (cm)	Top (cm)	Bottom (cm)	Thickness (cm)	Top (cm)	Bottom (cm)	Isopach (cm)
Quijada	PC1001A	78	T3 95	T4 73				
	PC1001B	85	T3 45	T4 30				
	PC1001C	Deformed			20	T2 15	T2 35	20
	PC1001D	88	T10 50	T11 38	20	T2 60	T2 78	20
Churrasco	PC1201A	65	T6 5	T6 70	18	T2 10	T2 28	20
	PC1201B	60	T6 60	T7 20	18	T1 60	T1 68	20
Unco	PC1103D	60	T8 30	T8 90	12	T3 10	T3 22	10
	PC1103E	60	T8 78	T9 38	10	T3 58	T3 68	10
Mellizas	PC1106A	68	T7 0	T7 68	10	T2 95	T3 5	10
		60	T6 60	T7 20	10	T2 55	T2 65	
Toro	PC1002B	50	T6 95	T7 45	10	T3 0	T3 10	10
	PC1002C	35	T8 20	T8 55	7	T3 18	T3 25	10
Tranquilo	PC1203A	65	T11 75	T12 40	10	T5 0	T5 10	>5
	PC1203B	60	T10 75	T11 35	9	T4 35	T4 44	>5
	PC1203C	70	T5 0	T5 70	6	T2 42	T2 48	>5
	PC1203D	68	T4 70	T5 38	7	T2 11	T2 18	>5
Elida	PC1105B	18	T7 16	T7 28	12	T1 56	T1 68	10

Isopach thickness for H2 from Naranjo and Stern (1998)

and 20-nA probe current were used to analyze glass and mineral grains.

Strontium isotopic ratios were measured using a Finnigan-Mat 261 four-collector static Thermal Ionization Mass Spectrometer. Powdered samples were first dissolved in open containers in HF and $HC1O_3$. Replicate analyses of the SRM-987 standard in this mode yielded a mean $^{87}Sr/^{86}Sr$ of 0.71025 ±2 (2σ). Measured $^{87}Sr/^{86}Sr$ were corrected to SRM-987= 0.710299±8. Errors of 2σ of the mean refer to the last two digits of the $^{87}Sr/^{86}Sr$ ratio. Details of the analytical procedure are outlined in Farmer et al. (1991).

Results

General

The length of the sediment record for the seven lakes with Ho tephra is variable, but these lakes each contain sediments that date back to late-glacial time (Miranda et al. 2013). The individual cores all preserve >50 to 74 distinct tephra layers derived from explosive eruptions of volcanoes in the area (Figs. 3 and 4). Based on their trace-element chemistry (Fig. 5) and their stratigraphic depth within the cores, specific source volcanoes for some of the Holocene eruptions have been identified (Figs. 3 and 4). These include the previously identified and dated large explosive H2 eruption of Hudson at ~3,920 cal years BP (Naranjo and Stern 1998) and MEN1 of Mentolat at 7,560 cal years BP (Naranjo and Stern 2004; Stern et al. 2013). Other chemically distinctive tephra from late-glacial eruptions that have not been previously described, such as a sequence of nine thin tephra layers dated as <14,910 cal years BP (S9; Figs. 3 and 4) and tephra from a previously undocumented late-glacial Mentolat eruption (MENo), with chemistry (Fig. 5), mineralogy, and glass color and morphology similar to MEN1, are preserved in all or most of the cores and allow late-glacial strato-chronologic correlations between the cores.

Ho deposits

Fifteen cores from the seven lakes studied contain an unusually thick tephra deposit, which provides evidence of a very large late-glacial explosive eruption. Based on their bulk trace-element composition (Fig. 5), discussed in more detail below, and their spatial distribution (Fig. 6), these deposits were derived from a large late-glacial eruption of the Hudson volcano. We term this eruption Ho (Weller et al. 2013). In three cores from Lago Quijada (Fig. 3), the closest to Hudson volcano (Fig. 2), the Ho layer ranges from 78 to 88 cm in thickness. In ten of the 11 cores from five other lakes, all ≥100 km northeast of the Hudson volcano, the Ho tephra layer ranges between 50 and 70 cm in thickness (Fig. 5; Table 2). Only in one of the cores, from Lago Toro, is Ho less than 50-cm thick (Table 2). Pumice size was not systematically

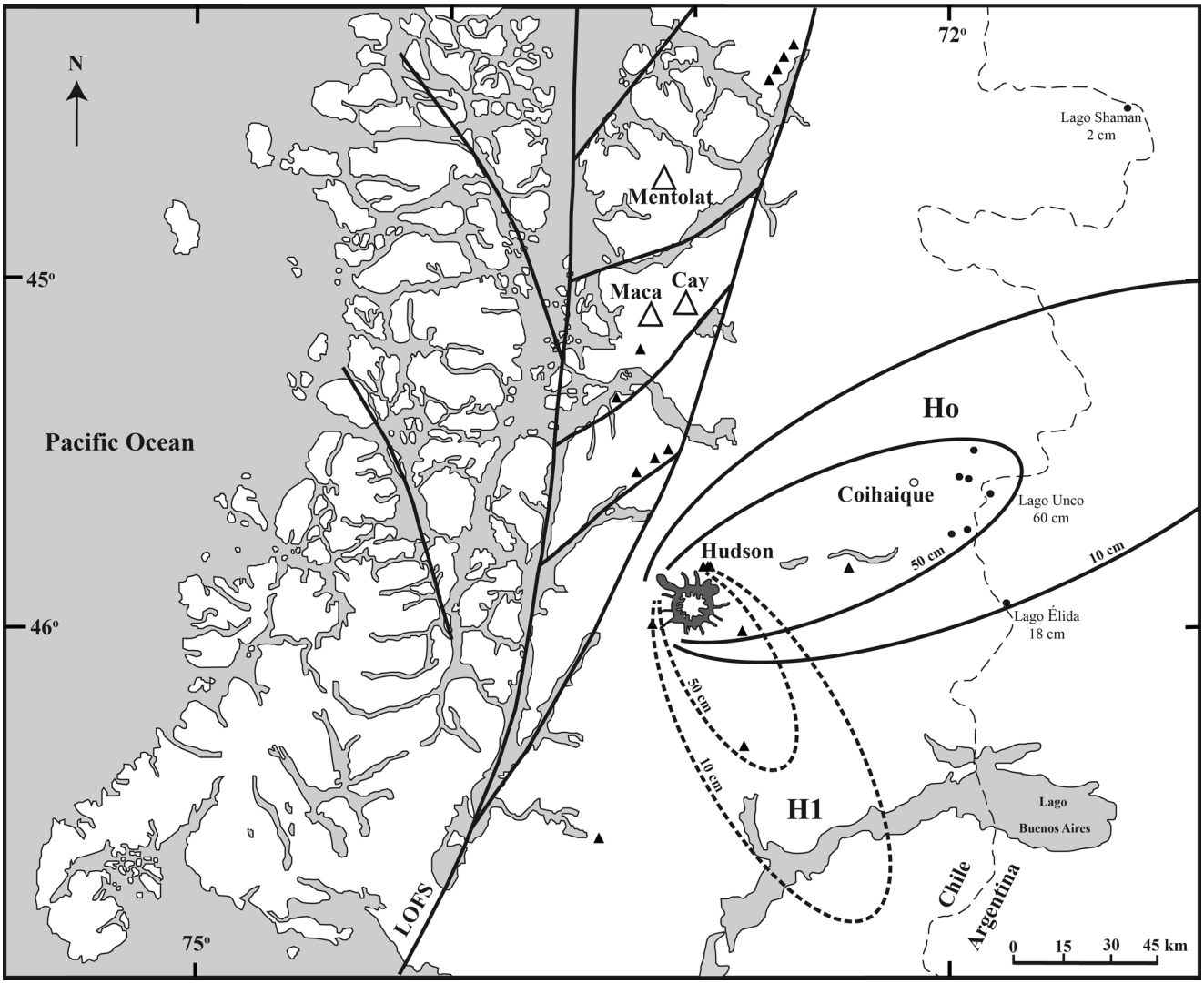

Fig. 6 Estimated 50- and 10-cm isopachs of the Ho eruption (*solid lines*) compared to those for the mid-Holocene H1 eruption (*dashed lines*; Naranjo and Stern 1998). The distribution of the Ho tephra indicates northeastward dispersion

measured in any of the cores, but the bulk samples obtained from the cores for petrochemistry contain Ho pumice grains up to 2 cm in maximum diameter. In a core from the seventh lake, Lago Élida (Figs. 1 and 2), more to the east of Hudson, and southeast of the other lakes, Ho is only 18-cm thick (Fig. 4; Table 2) and all pumice grains are <1 cm in maximum diameter. In another core from Lago Shaman (LS; Fig. 1) more than 200 km to the northeast, a 2-cm-thick late-glacial tephra (tephra V), one among 26 tephra identified in this core (de Porras et al. 2012), has tephra color, morphology, and chemistry (Fig. 5; Table 3) similar to Ho.

Both over-thickening and/or compaction of tephra fall deposits may occur in lake sediments. However, 15 of the cores from the lakes that contain Ho tephra also contain layers of H2 tephra that are similar in thickness to the regionally mapped isopachs for this tephra (Table 2; Naranjo and Stern 1998), suggesting that over-thickening was not a problem for this younger tephra in these small lake basins. Based on this as well as the lack of evidence for mixing of other sediment types within the Ho layers and the consistency of the thickness of the Ho layers both in different cores taken from different locations and depths in individual lakes and among the different lakes, we conclude that the Ho layers in these lakes have also not been significantly thickened.

Tentative 50- and 10-cm tephra isopachs for the Ho eruption are presented in Fig. 6 and compared to the 50-cm and the 10-cm tephra isopachs from the H1 eruption (Naranjo and Stern 1998). The area of these isopachs (Fig. 7) indicates that the late-glacial Ho eruption was larger than any of the other, younger, explosive eruptions of Hudson (H1, H2, or H3 in 1991 AD), and we estimate that its tephra volume exceeds 20 km^3.

Table 3 Trace-element composition (in ppm) of bulk samples of Ho

Lake	Churrasco	Tranquilo	Unco	Toro	Elida	Shaman
Section	AT6	AT12	ET9	BT7	BT7	AT7
Depth (cm)	67–74	0–40	0–3	34–37	10–28	6–8
Phase	Bulk	Bulk	Bulk	Bulk	Bulk	Bulk
Ti	8,365	8,346	7,810	8,150	10,508	7,366
V	240	212	175	187	309	–
Cr	15	21	17	13	34	–
Mn	1,182	1,157	1,097	1,161	1,260	890
Co	29	30	26	48	47	–
Ni	18	21	13	35	29	–
Cu	69	51	67	30	68	–
Zn	112	109	114	119	108	–
Rb	39	43	47	47	27	44
Sr	458	467	448	430	486	399
Y	31	31	34	33	31	29
Zr	203	222	275	261	184	213
Nb	11	13	22	16	10	10
Cs	1.5	1.5	1.4	1.3	0.7	1.0
Ba	479	537	584	586	373	480
La	26.4	29.4	32.7	32.5	23.3	28.0
Ce	58.2	64.9	71.0	70.7	53.7	63.2
Pr	7.48	8.23	8.95	8.55	7.01	7.61
Nd	31.9	34.1	36.3	35.3	29.9	31.1
Sm	7.21	7.57	7.76	7.35	6.71	6.49
Eu	2.16	2.29	2.31	2.35	2.10	1.79
Gd	8.26	8.61	8.89	9.00	7.80	7.37
Tb	1.09	1.10	1.21	1.05	1.02	0.88
Dy	5.80	5.87	6.03	6.11	5.84	5.24
Ho	1.14	1.17	1.20	1.16	1.11	0.94
Er	3.45	3.50	3.61	3.52	3.46	3.12
Tm	0.44	0.44	0.47	0.43	0.43	0.38
Yb	3.03	3.14	3.34	3.38	2.92	2.97
Lu	0.47	0.47	0.50	0.43	0.45	0.35
Hf	5.2	6.0	6.9	6.5	4.4	6.9
Pb	8.7	9.3	10.3	10.0	5.4	8.8
Th	4.8	5.7	8.1	6.1	3.7	4.6
U	1.1	1.2	1.3	1.5	0.9	1.3

The age of the Ho tephra layer has been inferred using ^{14}C methods to date organic matter located in sedimentary layers just above and below this tephra in the cores (Table 1; Miranda et al. 2013). This provides an age for this eruption of between 17,300 and 17,440 cal years BP. This age range is consistent with its stratigraphic position relative to other dated tephra in these cores (Fig. 3). Late-glacial tephra HW1 (14,560 cal years BP) and HW2 (13,890 cal years BP) documented by Haberle and Lumley (1998) from the Taitao Peninsula to the southwest of the Hudson volcano appear to be too young to be distal Ho tephra, and also occur in the opposite direction of the northeastern dispersal direction of Ho (Fig. 6).

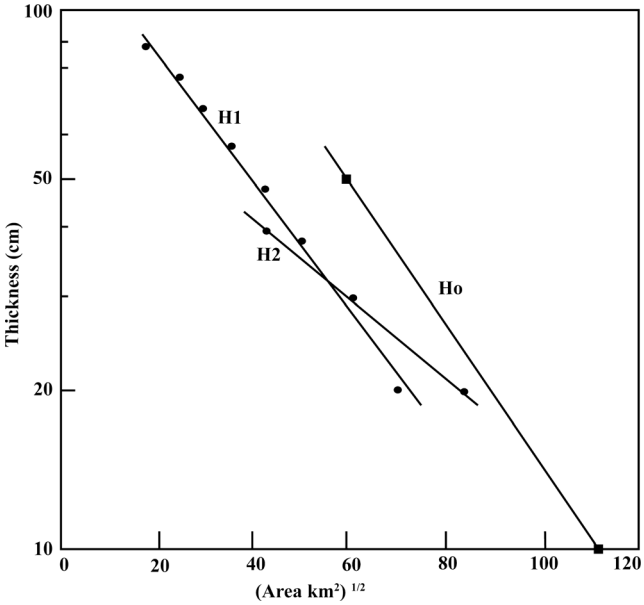

Fig. 7 Thickness (cm) versus (Area $km^2)^{1/2}$ of tephra from the H1, H2 (Naranjo and Stern 1998), and Ho eruptions

Bulk tephra chemistry

All of the bulk tephra trace-element analytical results (Table 3) are similar to each other and occupy a narrow range of trace-element chemistry characteristic of samples of lavas, pumice, and bulk tephra from other eruptions of Hudson volcano (Fig. 5). They have elevated concentrations of Ti (>7,000 ppm), Rb (>30 ppm), Zr (>200 ppm), Nb (>12 ppm), Y (>30 ppm), Ba (>500 ppm), La (>30 ppm), and Yb (>4 ppm) relative to both more-mafic and felsic eruptions from other volcanoes in the region (Stern 1991, 2008; Naranjo and Stern 1998; Kratzmann et al. 2010).

Tephra components

Clast morphology, mineralogy, and composition

The Ho tephra layers contain a diversity of glass particle morphologies and color (Fig. 8). The different components identified include dark-grey to light-tan glassy vesicle-rich pumice, denser dark black, vesicle-poor glassy fragments with a blocky morphology, and isolated mineral grains. The different components are randomly mixed within the deposit, which does not exhibit any vertical stratification. This may be due in part to the deposition of these layers in lakes rather than as primary fall deposits.

The dense blocky black glass fragments themselves have a diversity of morphologies and textures, including fragments which contain few vesicles and few mineral microlites (Fig. 8) as well as fragments with higher abundances of spherical vesicles and olivine, plagioclase, and clinopyroxene microlites, along with minor

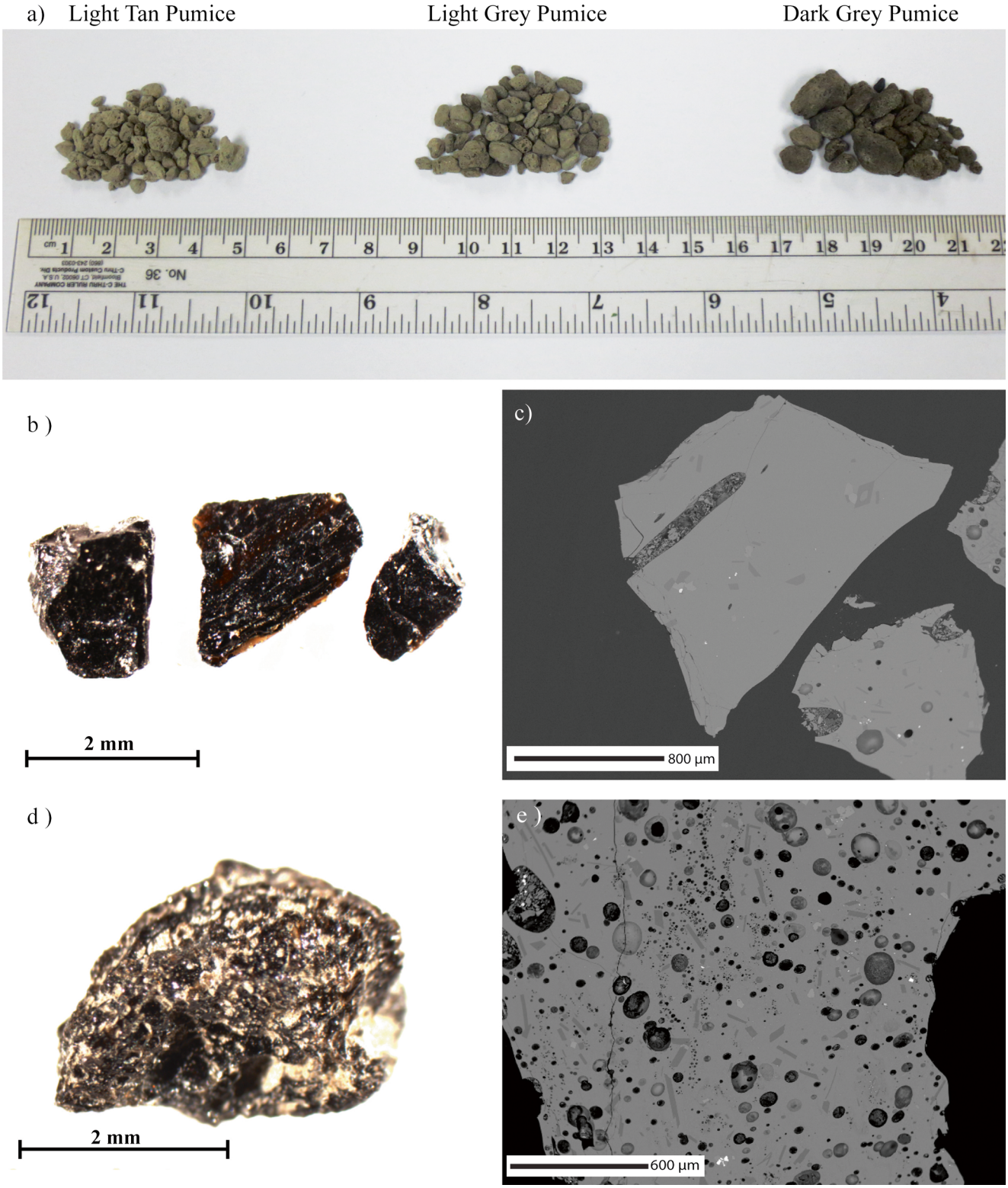

Fig. 8 Images of the different components identified in the Ho tephra deposit. **a** The three different color pumice groups selected from the deposit. The light-tan pumice contains glass with ~66 wt.% SiO_2 while the light- and dark-grey pumice contain glass with 59.3 % SiO_2 and 57.7 % SiO_2, respectively (Table 4). **b**, **d** Images of the nonvesicular and vesicular blocky dark glassy material. **c**, **e** Back-scattering electron images of the nonvesicular dense black glass with few mineral microlites and the more microlite-rich vesicular dark glassy material, respectively

ilmenite. These blocky dark glassy fragments are the most mafic basaltic-trachyandesite component from the Ho eruption (Table 4), with an average glass composition of 55 wt.% SiO_2 (Fig. 9), higher bulk Ti, Mn, and

Table 4 Major and trace-element (in ppm) compositions of selected Ho components

Lake	Churrasco	Mellizas	Tranquilo	Elida	Mellizas	Mellizas	Mellizas
Section	AT6	AT7	AT12	BT7	AT7	AT7	AT7
Depth (cm)	67–74	0–15	0–40	10–17	0–15	0–15	0–15
n	5	1	1	1	6	9	2
Phase	Black glass	Black glass	Black glass	Black glass	Dark-grey pumice	Light-grey pumice	Light-tan pumice
SiO_2	54.95	–	–	–	57.66	59.30	65.75
TiO_2	2.03	–	–	–	1.73	1.60	0.90
Al_2O_3	15.70	–	–	–	15.89	15.91	15.48
FeO	9.09	–	–	–	7.99	7.10	4.35
MnO	0.18	–	–	–	0.16	0.17	0.14
MgO	3.52	–	–	–	2.99	2.52	1.08
CaO	6.90	–	–	–	5.87	5.24	2.56
Na_2O	5.30	–	–	–	5.21	5.54	6.64
K_2O	1.54	–	–	–	1.83	2.04	2.90
P_2O_5	0.80	–	–	–	0.67	0.59	0.21
Total	100	–	–	–	100	100	100
Ti	11,527	8,995	8,257	11,121	10,311	8,620	5,940
V	340	252	215	328	254	195	104
Cr	61	24	15	32	15	12	13
Mn	1,343	1,173	1,091	1,366	1,284	1,181	1,017
Co	27	14	15	26	56	75	30
Ni	46	17	21	34	16	17	16
Cu	204	31	34	38	42	39	30
Zn	133	133	106	120	121	114	111
Rb	34	43	44	22	45	51	64
Sr	525	440	392	487	459	399	290
Y	32	33	33	31	36	36	38
Zr	182	263	228	175	260	287	362
Nb	9	13	12	8	13	15	18
Cs	0.6	-	1.2	-	1.1	1.3	1.7
Ba	456	502	487	306	559	604	720
La	35.0	34.7	31.7	24.3	34.5	34.9	40.7
Ce	80.7	79.2	70.1	56.3	76.8	78.1	90.1
Pr	10.1	9.2	8.6	7.1	9.7	10.0	10.7
Nd	42.5	33.9	34.7	30.7	40.8	41.6	43.4
Sm	9.21	7.32	7.62	6.58	8.84	9.14	9.50
Eu	2.68	2.13	2.06	2.03	2.55	2.58	2.50
Gd	10.2	7.9	8.4	7.3	10.1	10.4	11.1
Tb	1.21	1.03	1.06	1.01	1.28	1.31	1.35
Dy	6.42	5.41	5.55	5.26	7.07	7.03	7.18
Ho	1.24	1.01	1.11	1.00	1.31	1.39	1.48
Er	3.81	3.13	3.33	3.13	4.17	4.41	4.38
Tm	0.41	0.27	0.41	0.32	0.50	0.52	0.60
Yb	2.92	2.79	2.75	2.65	3.50	3.80	4.05
Lu	0.46	0.40	0.45	0.37	0.54	0.56	0.64
Hf	4.7	5.5	5.3	3.9	6.2	7.2	8.6
Pb	12.1	8.1	10.0	5.3	9.3	10.5	13.4
Th	5.4	4.8	5.8	3.3	5.5	6.0	7.3
U	1.4	1.0	1.2	0.6	1.3	1.4	1.8

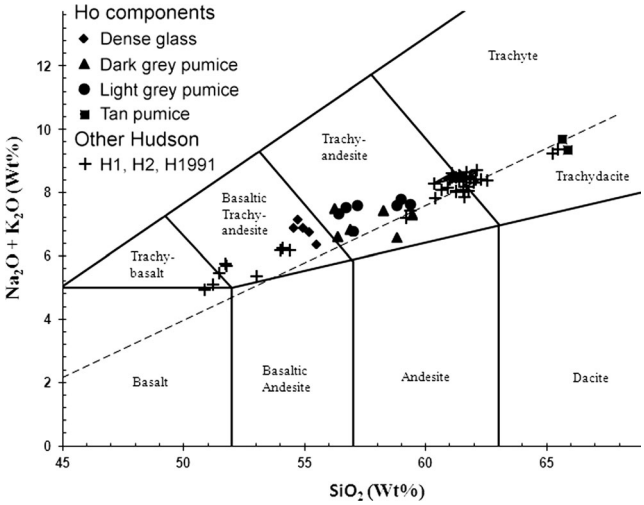

Fig. 9 Total alkali content versus silica diagram, modified after Irvine and Baragaar (1971), showing the range of compositions of the Ho tephra glasses. The *squares* represent the light-tan pumice, the *circles* represent the light-grey pumice, the *triangles* represent the dark-grey pumice, the *diamonds* represent the dark glassy vesicle-poor material in the Ho deposits, and the *plusses* represent glass from other Hudson eruptive products (Futa and Stern 1988; Naranjo and Stern 1998; Gutiérrez et al. 2005; Kratzmann et al. 2009, 2010)

Sr and lower Rb, Ba, Zr, La, and Yb contents, and higher Dy/Yb ratios (Fig. 10), than any pumice grains.

The small glassy pumice fragments prepared for microprobe analysis contain few or no mineral grains, or these grains were possibly plucked out during the polishing processes. Three separate groups were identified and hand-picked from the tephra deposits on the basis of color: dark grey, lighter grey, and light tan (Fig. 8). The glass in the dark- and lighter-grey pumice groups ranges only between 57.7 and 59.3 wt.% SiO_2 (Fig. 9; Table 4) despite their distinct color differences. Although the distinction between the major element chemistries between the glasses in the two grey pumice groups is minor, the bulk-pumice trace-element abundances show clear differences between the two components, with the lighter-grey phase having lower Ti, Mn, and Sr and higher Rb, Ba, and Zr contents, and lower Dy/Yb ratios (Fig. 10), than the dark-grey pumice. The lightest-tan-colored pumice is volumetrically less significant than the darker components, and its glass has an average trachydacite composition of 66 wt.% SiO_2 (Fig. 9), with even lower Ti, Mn, and Sr and higher Rb, Ba, Zr, and La contents and lower Dy/Yb ratios (Fig. 10). Thus, nearly the entire range of compositional diversity observed in the H3 Hudson eruption of 1991 AD (Kratzmann et al. 2009) is also present in the Ho tephra, and a similar compositional gap in groundmass glass as seen in the 1991 eruption is also present in the Ho eruption. However, the compositional gap between the dark- and lighter-colored pumice components in Ho glasses, which corresponds to ~7 wt.% between 59 and 66 wt.% SiO_2 occurs at a higher silica content than the gap in SiO_2 content in the 1991 Hudson eruption, which occurs between 54 and 60 wt.% SiO_2.

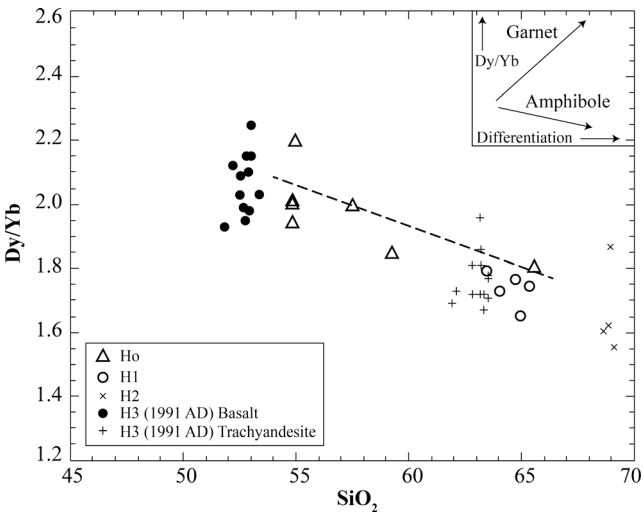

Fig. 10 Dy/Yb ratios of bulk Ho components versus their glass SiO_2 contents (Table 4) compared to the compositions of H1, H2, and H3 glasses plotted by Kratzmann et al. (2010). The *dashed line* from the average phase 1 basalt erupted in 1991, through the average Ho dense glass basaltic andesite to the Ho trachydacite pumice illustrates a small decrease in Dy/Yb with increasing SiO_2, indicative of amphibole fractionation as shown in the inset (Davidson et al. 2007), although amphibole does not occur in any of the Hudson eruptive products

Figure 9 plots total alkali content versus silica, showing the compositional classification of the various glass components from the Ho eruption. Included in this diagram are tephra from phase 1 and phase 2 of the H3 eruption in 1991 AD (Kratzmann et al. 2009) and other Hudson volcanic products (Futa and Stern 1988; Naranjo and Stern 1998; Gutiérrez et al. 2005). The glasses from the Ho eruption are high K_2O and range in composition from basaltic-trachyandesite to trachydacite. Like other Hudson eruptive products, they straddle the curve dividing the alkaline and subalkaline fields described by Irvine and Baragaar (1971).

The light-colored felsic pumice has a bulk $^{86}Sr/^{87}Sr$ ratio of 0.70445 and the more mafic vesicle-poor dark glassy material has a ratio of 0.70447 (Table 5). These isotopic compositions are very similar and coincide with the strontium isotopic ratios measured on all other bulk tephra and effusive rock samples from previous Hudson eruptions, which overall range in composition from 51 to 66 wt.% SiO_2 and 525 to 227 ppm Sr (Fig. 11; Futa and Stern 1988; Stern 1991, 2008; Naranjo and Stern 1998).

Mineral chemistry

Olivine microlites analyzed from the most mafic dark glassy fragments are generally anhedral to subhedral and commonly occur as aggregates with other microlites such as clinopyroxene, plagioclase, and Fe-Ti oxides. Analyzed olivines occupy a narrow compositional range of Fo75 to Fo67, with olivine microlites from Lago Élida (LÉl) being slightly

Table 5 Sr-isotopes and Sr and SiO_2 contents for bulk Ho components and H1, H2, and phase 1 (P1) of H3 in 1991 AD

Eruptive Event Material	Ho Tan pumice	Ho Dense glass	H3 P1 Ash	H2 Pumice	H2 Ash	H1 Pumice	H1 Ash	H1 Tephra	H1 Tephra	H1 Tephra	H-1 Lava
SiO_2 (wt.%)	65.75[a]	54.95[a]	51.12	64.3	65.12	369	61.88	61.88	61.76	60.61	52.79
Sr (ppm)	290	525	510	227	243	382	369	361	374	392	500
$^{87}Sr/^{86}Sr$	0.70445	0.70447	0.70437	0.70444	0.70445	0.70450	0.70451	0.70452	0.70451	0.70448	0.70449

Data for H1, H2, and H3 in 1991 AD from Naranjo and Stern (1998). Data for lava sample H-1 from Futa and Stern (1988)

[a] Glass composition

less MgO rich (Fo70–67) than the olivines in the blocky black glass separates from Lago Mellizas (LM) and Lago Churasco (LC; Table 6; Fig. 12). Clinopyroxene microlites in the dark glassy material also have a restricted range of En48–41, Wo43–35, Fs20–16, and clinopyroxene phenocrysts, which occur as large grains with some attached glass, occupy a similar compositional range En49–46, Wo35–27, and Fs23–19. Clinopyroxenes from LÉl are similar to those analyzed in both LM and LC (Table 6, Fig. 12). Olivine and clinopyroxene microlites observed in the fallout deposits from the H3 1991 AD eruption (Kratzmann et al. 2009), and other Hudson eruptive products (Gutiérrez et al. 2005; Kratzmann et al. 2010) share similar compositions to the mineral phases observed in Ho.

No orthopyroxene microlites were observed within the blocky glass fragments or pumice, but orthopyroxene phenocrysts were found as large isolated grains mixed within the bulk tephra deposits. The majority of these crystals are elongate euhedral grains with some adhering glass. They have a restricted compositional range of En61-59, Wo4-3, and Fs38-36 (Table 6; Fig. 12). Orthopyroxene with similar chemistry also occurs in H1 and H2 deposits and was reported as well in trace amounts from the H3 trachydacite tephra (Kratzmann et al. 2009, 2010).

Plagioclase occurs both as microlites contained in the dark blocky mafic glass fragment and also as larger phenocrysts, which like orthopyroxenes have become dislodged from the pumice and tephra in the bulk deposits, but still have glass adhering to their crystal surfaces. Plagioclase microlites within the black glassy fragments are generally euhedral to subhedral and are the dominant microlite observed in this mafic component of the tephra deposit. They have a narrow compositional range of An51–58 (Table 7; Fig. 13) with most of the grains being unzoned. The larger plagioclase phenocrysts occupy a larger compositional range of An41–55 and also have no core-to-rim variation. Included in Fig. 13 are plagioclase compositions from other Hudson volcanic products (Gutiérrez et al. 2005; Kratzmann et al. 2009, 2010), which span a wide range of compositions, with the largest population clustering near the composition of the plagioclase microlites and phenocrysts in the Ho tephra.

Discussion

Hudson eruptive history

The distribution of the Ho tephra across the area indicates a northeast dispersion pattern of the ash fall with a maximum thickness of 88 cm at a distance of ~100 km from the source vent (Figs. 2 and 6). Based on comparison with all of the three previously documented large Holocene Hudson eruptions H1, H2, and H3 in 1991 AD (Stern 1991, 2008; Scasso et al. 1994; Naranjo and Stern 1998), Ho is larger, with an estimated volume of >20 km^3 (Fig. 7) of pyroclastic material. This eruption may have caused or initiated the incremental formation of Hudson's 10-km-wide summit caldera. The data suggest a sequential temporal decrease in the total volume of each large explosive eruption, from Ho >20 km^3, to H1 > 18 km^3, to

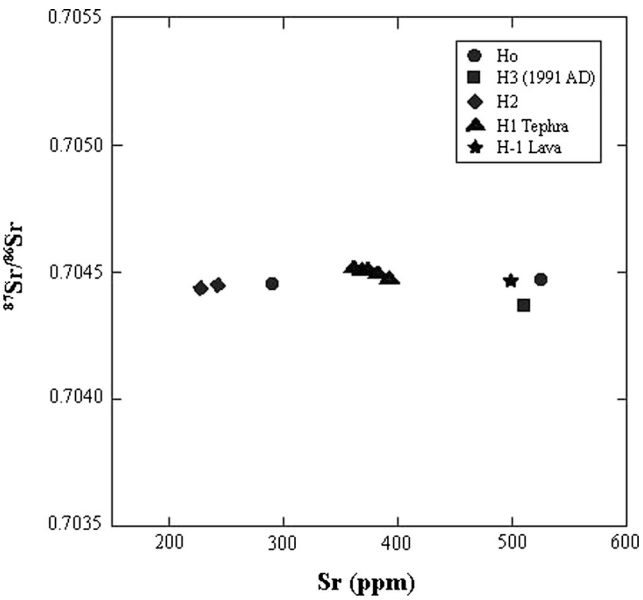

Fig. 11 $^{87}Sr/^{86}Sr$ ratios versus Sr content for components from the Ho eruption (circles; Table 5), and bulk rock samples from phases 1 and 2 of H3 in 1991 AD (*square*), H1 (*triangles*), H2 (*diamonds*) eruptions (Naranjo and Stern 1998; Stern 1991, 2008), and a basaltic andesite lava sample H-1 from the base of the volcano (Futa and Stern 1988)

Table 6 Compositions of olivines and pyroxenes in the Ho deposits

Lake	Section	Depth (cm)	Phase	SiO_2	TiO_2	Al_2O_3	Fe_2O_3	MnO	MgO	CaO	Na_2O	Total	En	Wo	Fs	Fo	Fa
LM	AT7	0–15	ol	37.91	0.07	0.04	23.94	0.39	36.05	0.35	–	98.8	–	–	–	73	27
LC	AT6	67–74	ol	37.73	0.06	0.02	25.50	0.43	34.92	0.26	–	98.9	–	–	–	71	29
LC	AT6	67–74	ol	37.81	0.04	0.00	24.83	0.46	35.85	0.18	–	99.2	–	–	–	72	28
LC	AT6	67–74	ol	38.74	0.06	0.01	22.42	0.45	37.76	0.27	–	99.7	–	–	–	75	25
LC	AT6	67–74	ol	37.71	0.04	0.03	25.07	0.45	36.68	0.23	–	100.2	–	–	–	72	28
LEl	BT7	10–17	ol	36.67	0.11	0.34	26.35	0.47	33.86	0.48	–	98.3	–	–	–	70	30
LEl	BT7	10–17	ol	36.25	0.07	0.10	28.64	0.57	32.12	0.28	–	98.0	–	–	–	67	33
LM	AT7	0–15	cpx	49.93	1.60	4.08	13.48	0.35	15.98	12.36	0.31	98.1	49	27	23	–	–
LM	AT7	0–15	cpx	49.15	1.43	3.90	11.36	0.39	15.43	16.56	0.42	98.7	46	35	19	–	–
LC	AT6	67–74	cpx	48.27	1.62	4.16	10.14	0.24	14.40	19.38	0.36	98.6	42	41	17	–	–
LC	AT6	67–74	cpx	48.06	1.84	4.54	11.65	0.39	15.27	16.30	0.38	98.4	46	35	19	–	–
LC	AT6	67–74	cpx	47.06	2.01	4.90	9.60	0.27	13.42	19.79	0.36	97.4	41	43	16	–	–
LC	AT6	67–74	cpx	51.41	0.72	1.63	10.26	0.29	16.29	16.63	0.21	97.5	48	35	17	–	–
LEl	BT7	10–17	cpx	47.73	2.01	4.58	10.92	0.30	13.44	18.09	0.48	97.5	41	40	19	–	–
LEl	BT7	10–17	cpx	49.20	1.71	3.68	11.72	0.37	15.67	15.83	0.34	98.5	47	34	20	–	–
LM	AT7	0–15	opx	51.65	0.19	0.47	23.23	1.32	20.29	1.66	–	98.8	59	3	38	–	–
LM	AT7	0–15	opx	51.65	0.17	0.38	23.07	1.31	21.01	1.71	-	99.3	60	3	37	–	–
LM	AT7	0–15	opx	53.23	0.30	0.56	22.17	1.22	21.41	1.64	-	100.6	61	3	36	–	–

H2 and finally H3 in 1991 AD with only ≥4 km^3 (Fig. 14), and supports the suggestion of Watt et al. (2013) that deglaciation resulted in generally increased volcanic activity compared to the present.

Adding the total estimated volumes of Ho to that of the previously documented eruptions H1, H2, and H3 in 1991 AD, as well as of at least 11 smaller eruptions (Fig. 14), shows that ≥45 km^3 of pyroclastic material has been erupted from Hudson in the last ~17,500 years (Fig. 14). This would make Hudson the most productive volcano in the southern Andes in terms of total volume of pyroclastic material erupted by explosive eruptions since the beginning of deglaciation at approximately 17,900 cal years BP.

Petrogenesis

An interesting distinction between the Ho eruption and the H3 eruption in 1991 AD is the lack of stratification of the Ho deposits with regard to the size or composition of the distinct components in the deposit, even though both eruptions contain bimodal eruptive products. The H3 eruption had a clear temporal distinction between the two chemically different

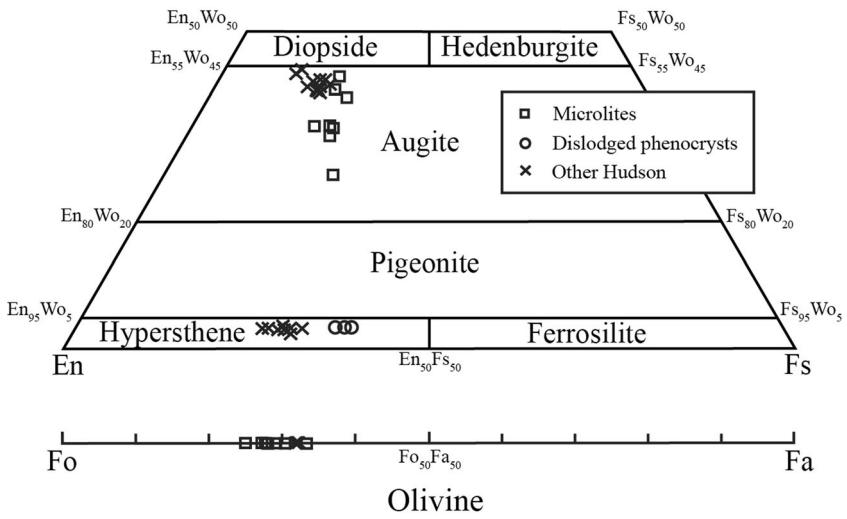

Fig. 12 Wo-En-Fs classification diagram for pyroxenes and olivines. Clinopyroxene and olivines are present as microlites in dense black glassy fragments, while the orthopyroxene and some clinopyroxenes occur as large dislodged phenocrysts with some adhering glass. Other Hudson mineral analysis from Gutiérrez et al. (2005) and Kratzmann et al. (2009, 2010)

Table 7 Electron microprobe analysis of representative plagioclase micolites and phenocrysts from the Ho eruption

Lake	Section	Depth (cm)	Mineral type	SiO_2	Al_2O_3	FeO	CaO	Na_2O	K_2O	MgO	Total	An	Ab	Or
LM	AT7	0–15	Grains	54.30	29.69	0.82	11.13	4.88	0.21	0.10	101.1	55	44	1
LM	AT7	0–15	Grains	54.76	28.74	0.96	10.73	4.89	0.30	0.16	100.5	54	44	2
LM	AT7	0–15	Grains	58.09	26.03	1.09	8.00	6.16	0.49	0.11	100.0	41	57	3
LC	AT6	67–74	Microlites	53.02	29.73	0.88	11.33	4.56	0.18	0.11	99.8	57	42	1
LC	AT6	67–74	Microlites	55.70	28.83	0.91	10.23	5.29	0.23	0.11	101.3	51	48	1
LC	AT6	67–74	Microlites	52.68	29.47	0.96	11.59	4.57	0.17	0.15	99.6	58	41	1
LC	AT6	67–74	Microlites	54.65	28.79	0.88	10.57	5.17	0.21	0.11	100.4	52	46	1
LC	AT6	67–74	Microlites	54.25	29.65	0.75	11.03	4.95	0.21	0.11	101.0	55	44	1
LC	AT6	67–74	Microlites	53.51	29.34	0.59	10.97	4.96	0.18	0.08	99.6	54	45	1
LEl	BT7	10–17	Microlites	59.41	21.86	0.38	6.88	6.09	0.43	0.04	95.1	37	60	3
LEl	BT7	10–17	Microlites	58.79	26.00	0.35	6.97	7.03	0.42	0.03	99.6	35	63	2
LEl	BT7	10–17	Microlites	56.31	27.97	0.86	9.53	5.49	0.30	0.09	100.6	48	50	2

phases as the eruption evolved from basalt and basaltic andesite in phase 1 to trachydacite and trachyandesite in phase 2. The genetic relationship between the two phases has been attributed to a combination of magma mixing and fractional crystallization (Kratzmann et al. 2009), who suggested that fractional crystallization of plagioclase (7.8–18.0 %), clinopyroxene (4.8–11.6 %), orthopyroxene (1.9–6.9 %), magnetite (2.9–6.7 %), and apatite (0.5–1.5 %) from a mafic parental magma similar to the P1 basalt is capable of generating magma with a trachydacite composition similar to the dominant tephra observed in phase 2. Kratzmann et al. (2010) subsequently presented similar fractional crystallization models, involving the anhydrous phases observed in the eruption products, for producing the H1 and H2 trachyandesites and trachydacites from a basalt similar to that erupted during phase 1 of the H3 eruption in 1991 AD. However, they further suggested that trace-element concentrations and ratios, specifically decreasing Dy/Yb ratio trends through the sequence basalts, trachyandesites, and trachydacites erupted in these three eruptions (Fig. 10), could be better explained by amphibole fractionation from a basalt parent at >6-km depth (Davidson et al. 2007), followed by disappearance of amphibole, due to decreasing pressure and

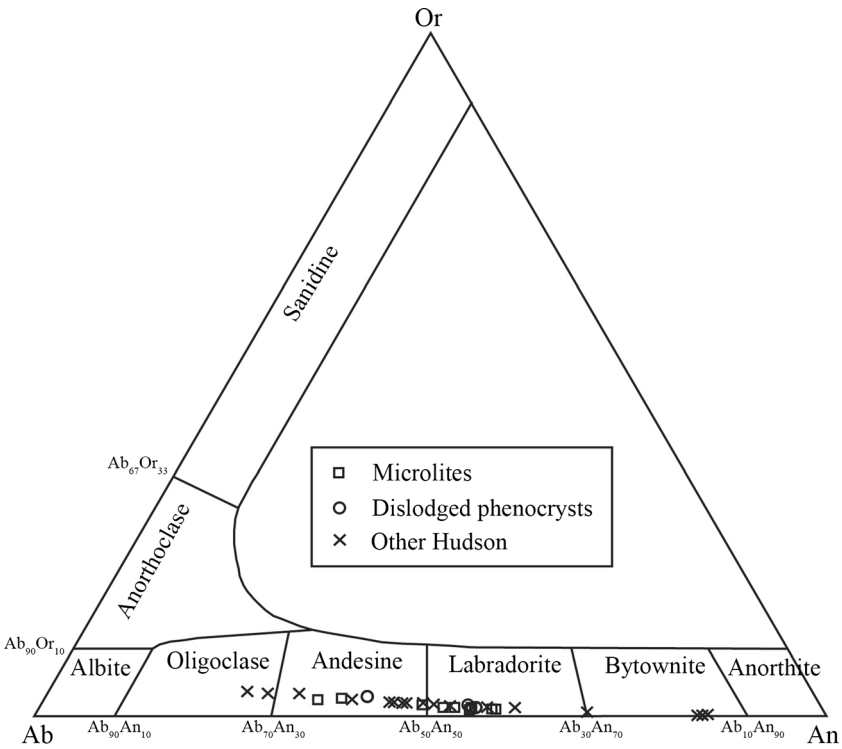

Fig. 13 Ab-An-Or compositional triangle for feldspar microlites in dense dark glassy fragments and for large dislodged phenocryst. Other Hudson mineral analysis from Gutiérrez et al. (2005) and Kratzmann et al. (2009, 2010)

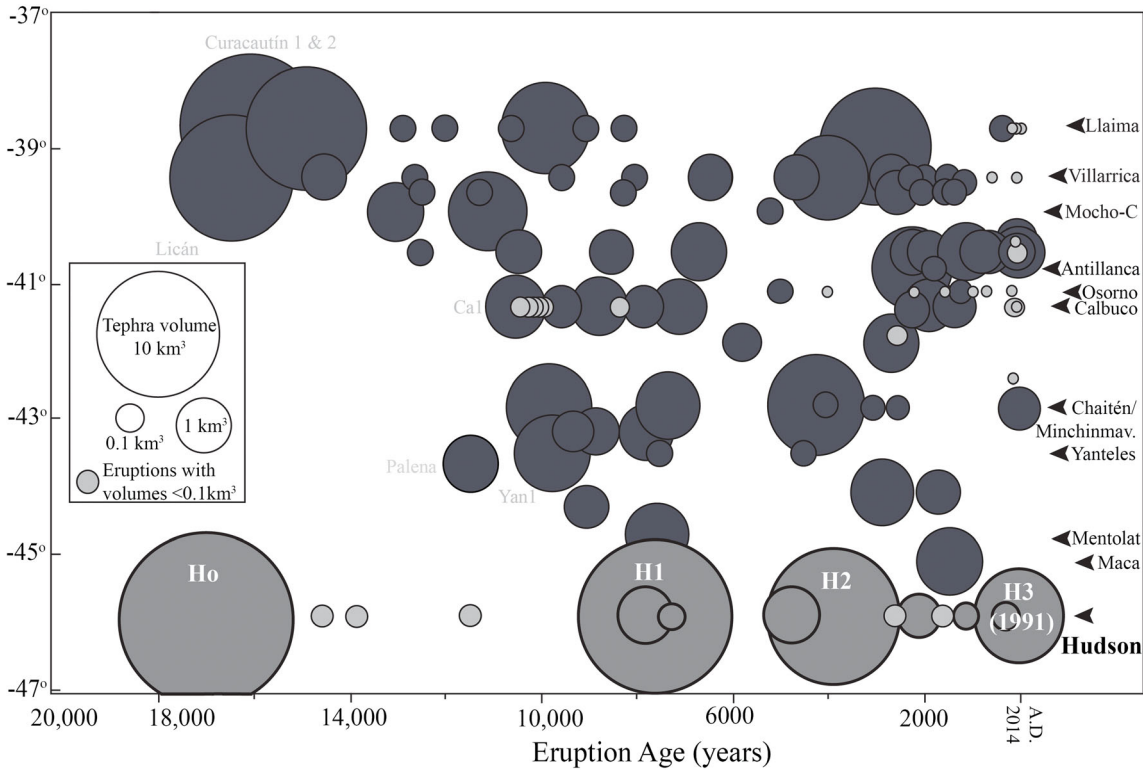

Fig. 14 Volumes produced by explosive eruptions of different late-glacial and Holocene ages (cal years BP) from volcanoes in the southern SVZ between latitudes 39°S (Llaima) and 46°S (Hudson), modified from Watt et al. (2013) to include the large late-glacial Ho eruption from Hudson (>20 km^3). Hudson volcano, with four large explosive eruptions and at least 11 other smaller explosive events, totaling >45 km^3 volume over the last 17,500 years, has produced the greatest volume of explosive eruptive products in the SSVZ over this time period

increasing temperature, as a result of decompression crystallization, as these magmas rose toward the surface. Ho components exhibit similar Dy/Yb ratio trends (Fig. 10) consistent with this latter cryptic amphibole fractionation model.

The strontium isotope ratios of the mafic dark glassy fragments and the felsic light-tan pumice in the Ho tephra deposits, as well as all the other analyzed extrusive units from the Hudson volcano, which overall range in SiO_2 from 51 to 66 wt.%, show almost no variation (Fig. 11; Table 5). The homogenous isotopic composition between the different samples is consistent with the suggestion of Kratzmann et al. (2009, 2010) that the evolution of Hudson magmas are controlled by fractional crystallization processes and that crustal assimilation is not responsible for the generation of the more evolved phases observed in either the H3 eruption in 1991 or any of the other documented Hudson eruptions. It is likely that crystal-liquid fractionation process similar to those suggested by Kratzmann et al. (2009, 2010) for the H1, H2, and H3 eruptions controlled the evolution of the Ho eruptive products, which also range from basaltic-trachyandesite to trachydacite in composition.

The Ho deposits are overall dark in color, with a much greater abundance of mafic dark glass fragments and dark- to light-grey pumice compared to light-tan felsic pumice. The bulk tephra trace-element abundances (Table 3), which are a representative portion of each deposit, can also be used to evaluate the relative proportions of mafic and felsic components (Table 4) in this deposit. Based on the comparison of the bulk-tephra, dense glassy material, and the pumice chemical analysis, the compositions of the bulk-tephra samples (Table 3) are more similar to that of the darker, more mafic dense glass and pumice components, confirming that the eruption was predominantly of relatively mafic basaltic-trachyandesite with only a smaller portion of more felsic trachydacite material. Thus, although Ho at ~17,400 cal years BP was bi-modal, it erupted a much greater proportion of mafic basaltic-trachyandesite compared to more felsic material. H1 at 7,750 cal years BP was essentially trachyandesitic in composition (Naranjo and Stern 1998). H2 at 3,960 cal years BP was more felsic than H1, being composed essentially of trachydacite. H3 in 1991 AD was again bi-modal, but with a much smaller proportion of mafic basalt compared to felsic trachydacite material (Kratzmann et al. 2009). We conclude that the large explosive eruptions of Hudson have evolved on average from more to progressively less mafic through late-glacial to historic times, and their volumes have decreased.

Acknowledgments We thank M. Kaplan, M. Fletcher, I. Villanova, W. Henriquez, and E. Simi for the assistance in the field obtaining the cores. J. Muñoz, S. Watt, and Associate Editor M. Coombs provided constructive comments that helped improve the final manuscript. This research was supported by Fondecyt (Chile) grant #1121141, the Institute of Ecology and Biodiversity grants ICM P05–002 and PFB-23, and the Department of Geological Sciences, CU-Boulder. We also would like to thank A. Vichick, T. Nightingale, M., D.T., D.R, and D.T. Weller for their continued support.

References

Auer V (1974) The isorythmicity subsequent to the Fuego-Patagonian and Fennoscandian ocean level transgressions and regressions of the latest glaciation. Ann Acad Sci Fenn (Hels) Ser A III Geol Geogr 115:1–188

Best JL (1989) Fluidization pipes in volcaniclastic mass flows, Volcán Hudson, southern Chile. Terra Nova 1:203–208

Best JL (1992) Sedimentology and event timing of a catastrophic volcaniclastic mass flow, Volcán Hudson, southern Chile. Bull Volcanol 54:299–318

Cande SC, Leslie RB (1986) Late Cenozoic tectonics of the southern Chile trench. J Geophys Res 91(B1):471–496

Cembrano J, Hervé F, Lavenu A (1996) The Liquiñe-Ofqui fault zone: long-lived intra-arc fault system in southern Chile. Tectonophysics 259:55–66

Cevo J (1978) Informe preliminar sobre erupción del Volcán Hudson norte o Volcán Huemules. Trapananda 1:35–42

D'Orazio M, Innocenti F, Manetti P, Tamponi M, Tonarini S, González-Ferrán O, Lahsen A (2003) The Quaternary calc-alkaline volcanism of the Patagonian Andes close to the Chile triple junction: geochemistry and petrogenesis of volcanic rocks from the Cay and Maca volcanoes (~45°S, Chile). J South Am Earth Sci 16(4):219–242

Davidson J, Turner S, Handley H, Macpherson C, Dosseto A (2007) Amphibole "sponge" in arc crust? Geology 35(9):787–790

de Porras ME, Maldonado A, Abarzúa AM, Cárdenas ML, Francois JP, Martel-Cea A, Stern CR (2012) Postglacial vegetation, fire and climate dynamics at Central Chilean Patagonia (Lake Shaman, 44°S). Quat Sci Rev 50:71–85

Farmer GL, Broxton DE, Warren RG, Pickthorn W (1991) Nd, Sr, and O isotopic variations in metaluminous ash-flow tuffs and related volcanic rocks at Timber Mountain/Oasis Valley Caldera, Complex, SW Nevada: implication for the origin and evolution of large-volume silicic magma bodies. Contrib Mineral Petrol 109:53–68

Fuenzalida RP (1976) The Hudson volcano. Proceedings of the IAVCEI symposium on Andean and Antarctic volcanology problems, 1974, Santiago, Chile pp 78–87

Fuenzalida RP, Espinosa WN (1974) Hallazgo de una caldera volcánica en la provincia de Aisén. Rev Geol Chile 1:64–66

Futa K, Stern CR (1988) Sr and Nd isotopic and trace element compositions of Quaternary volcanic centers of the southern Andes. Earth Planet Sci Lett 88:253–262

Gutiérrez F, Gioncada A, Gonzalez-Ferran O, Lahsen A, Mazzuoli R (2005) The Hudson volcano and surrounding monogenetic centres (Chilean Patagonia): an example of volcanism associated with ridge-trench collision environment. J Volcanol Geotherm Res 145:207–233

Haberle SG, Lumley SH (1998) Age and origin of tephras recorded in postglacial lake sediments to the west of the southern Andes, 44°S to 47°S. J Volcanol Geotherm Res 84:238–256

Hildreth W, Drake RE (1992) Volcán Quizapu, Chilean Andes. Bull Volcanol 54:93–125

Irvine TN, Baragaar WRA (1971) A guide to the chemical classification of the common volcanic rocks. Can J Earth Sci 8(5):523–548

Kratzmann DJ, Carey S, Scasso RA, Naranjo JA (2009) Compositional variations and magma mixing in the 1991 eruptions of Hudson volcano, Chile. Bull Volcanol 71(4):419–439

Kratzmann DJ, Carey S, Scasso RA, Naranjo JA (2010) Role of cryptic amphibole crystallization in magma differentiation at Hudson volcano, Southern Volcanic Zone, Chile. Contrib Mineral Petrol 159: 237–264

López-Escobar L, Kilian R, Kempton P, Tagiri M (1993) Petrology and geochemistry of Quaternary rocks from the southern volcanic zone of the Andes between 41°30′ and 46°00′S, Chile. Rev Geol Chile 20:33–55

Miranda CG, Moreno PI, Vilanova I, Villa-Martinez RP (2013) Glacial fluctuations in the Coyhaique-Balmaceda sector of central Patagonia (45S-46S) during the last glacial termination. Boll Geofis Teor Appl 54(Supplement 2):268–271

Naranjo JA (1991) Nueva erupción del volcán Hudson. Rev Geol Chile 18:183–184

Naranjo JA, Stern CR (1998) Holocene explosive activity of Hudson Volcano, southern Andes. Bull Volcanol 59(4):291–306

Naranjo JA, Stern CR (2004) Holocene tephrochronology of the southernmost part (42°30′-45°S) of the Andean Southern Volcanic Zone. Rev Geol Chile 31(2):225–240

Naranjo JA, Moreno H, Banks NG (1993) La erupción del volcán Hudson 1991 (46°S), Región de Aisén, Chile. Serv Nac Geol Min Boletin 44:1–50

Nelson E, Forsythe R, Arit I (1994) Ridge collision tectonics in terrane development. J South Am Earth Sci 7(3–4):271–278

Orihashi Y, Naranjo JA, Motoki A, Sumino H, Hirata D, Anma R, Nagao K (2004) Quaternary volcanic activity of Hudson and Lautaro volcanoes, Chilean Patagonia: New constraints from K-Ar ages. Rev Geol Chile 31(2):207–224

Pankhurst RJ, Weaver SD, Hervé F, Larrondo P (1999) Mesozoic–Cenozoic evolution of the North Patagonian Batholith in Aysén, southern Chile. J Geol Soc 156:673–694

Prieto A, Stern CR, Esterves J (2013) The peopling fo the Fuego-Patagonian fjords by littoral hunter-gatherers after the mid-Holocene H1 eruption of Hudson Volcano. Quat Int 317:3–13

Scasso RA, Corbella H, Tiberi P (1994) Sedimentological analysis of the tephra from the 12–15 August 1991 eruption of Hudson volcano. Bull Volcanol 56:121–132

Stern CR (1991) Mid-Holocene tephra on Tierra del Fuego (54°S) derived from the Hudson volcano (46°S): evidence for a large explosive eruption. Rev Geol Chile 18:139–146

Stern CR (2004) Active Andean Volcanism: its geologic and tectonic setting. Rev Geol Chile 31(2):161–206

Stern CR (2008) Holocene tephrochronology record of large explosive eruptions in the southernmost Patagonian Andes. Bull Volcanol 70(4):435–454

Stern CR, Moreno H, López-Escobar L, Clavero JE, Lara LE, Naranjo JA, Parada MA, Skewes MA (2007) Chilean volcanoes. Chapter 5 in "The Geology of Chile" (T Moreno & W. Gibbons, eds), Geologic Society of London, pp 149–180

Stern CR, Kilian R (1996) Role of the subducted slab, mantle wedge and continental crust in the generation of adakites from the Andean austral volcanic zone. Contrib Mineral Petrol 123:263–281

Stern CR, Moreno PI, Henrique WI, Villa-Martinez RP, Sagredo E, Aravena JC (2013) Tehrochronolgy in the area around Cochrane, southern Chile. Boll Geofis Teor Appl 54(Supplement 2):199–202

Stuiver M, Reimer PJ, Braziunas TF (1998) High-precision radiocarbon age calibration for terrestrial and marine samples. Radiocarbon 40(3):1127–1151

Tobar A (1972) Event 80–71. l971 Annual Report, Smithsonian Institution, Center of short-lived phenomena, pp 105–109

Watt SFL, Pyle DM, Mather TA (2013) The volcanic response to deglaciation: evidence from glaciated arcs and a reassessment of global eruption records. Earth Sci Rev 122:77–102

Weller DJ, Stern CR, Miranda CG, Moreno PI, Villa-Martinez RP (2013) A very large (>20km^3) late-glacial eruption (Ho) of the Hudson volcaono, southern Chile. Boll Geofis Teor Appl 54(Supplement 2):203–206

Wilson TM, Cole JW, Stewart C, Cronin SJ, Johnston DM (2011) Ash storms: impacts of wind-remobilised volcanic ash on rural communities and agriculture following the 1991 Hudson eruption, southern Patagonia, Chile. Bull Volcanol 73:223–239

Wilson T, Cole J, Johnston D, Cronin S, Stewart C, Dantas A (2012) Short-and long-term evacuation of people and livestock during a volcanic crisis: lessons from the 1991 eruption of Volcan Hudson, Chile. J Appl Volcanol 1:2

Wright HE Jr (1967) A square-rod piston sampler for lake sediments. J Sed Petrol 37:975–976